Anal. Chem. **2002,** *74,* 3281−3289

Study of Layer-by-Layer Self-Assembled Viscoelastic Films on Thickness-Shear Mode Resonator Surfaces

Ernesto J. Calvo,* Erica S. Forzani, and Marcelo Otero

INQUIMAE, Departamento de Química Inorgánica, Analítica y Química Física, Facultad de Ciencias Exactas y Naturales, Universidad de Buenos Aires, Pabellón 2, Ciudad Universitaria, AR-1428 Buenos Aires, Argentina

We describe quartz crystal electroacoustic admittance studies in thickness shear mode resonators loaded with self-assembled multilayers composed of alternate layers of glucose oxidase (GOx) and poly(allylamine) covalently attached to $[Os(bpy)_2ClPyCOH]^-$, (PAH−Os), deposited on a 3-mercaptopropanesulfonic acid (MPS)-modified gold on the quartz crystal. The complex acoustic impedance parameters, R_S and X_{LS} of a lumped-element Butterworth−Van Dyke (BVD) resonator have been determined for organized thin films of different thickness obtained by varying the number of enzyme layers, n, in $(PAH−Os)_n(GOx)_n$ structures. The ellipsometric film thickness and mass for dry enzyme multilayer films and films in contact with water were evaluated, and the average film density was estimated. By combination of the estimated film thickness and density, the expression for the surface mechanical impedance of the lumped-element modified resonator (Granstaff and Martin model), and the liquid density and viscosity, we simulate the layer-by-layer film growth on the basis of the measured electroacoustic impedance. The complex impedance X_{LS} and R_S increase with film thickness and the enzyme films can be regarded as acoustically thin in the reduced state for films thinner than 600 nm. We have also measured electroacoustic parameters for PAH−Os/GOx self-assembled multilayers under electrochemical perturbation in a buffer electrolytic solution. The electrostatically self-assembled multilayers behaved as lossy viscoelastic films at 10 MHz with G'_f and G''_f on the order of 10^6 Pa. The films became viscoelastic upon oxidation to Os(III), resulting in an increase of R_S and X_{LS} in the oxidized state with the number of (PAH−Os)(GOx) bilayers due to film swelling and an increase in the shear moduli during oxidation.

Thickness shear mode (TSM) resonators are widely employed in sensors with a sensing thin film coating the quartz as a molecular recognition layer, which in many cases is a polymer or enzyme film.[1−5] Rigidly coupled films, that is, metal deposits on the quartz resonators, can be used as a gravimetric tool with the surface in air or exposed to vapors and the quartz crystal immersed in viscous liquids. In the latter case, the shear wave penetrates the surface film and is attenuated by viscous dissipation. For polymers deposited on quartz crystal resonators, the liquid may also swell the polymer, thereby increasing the acoustic thickness. In addition, the solvent penetrating into the film can act as a plasticizer, softening the polymer film and producing viscoelastic changes that complicate the interpretation of frequency response.[5−10]

Spatially organized protein layers in supramolecular multilayers can be obtained by consecutive electrostatic adsorption of positively and negatively charged polyelectrolytes and proteins, reversing the surface charge in every immersion step.[6−12]

Several authors have reported studies of protein layers on quartz crystal resonators, including frequency shift and shear energy dissipation.[13−20] The energy dissipation arise primarily from losses within the protein layer.

We have built layer-by-layer self-assembled enzyme films by alternate electrostatic adsorption of poly-(allylamine) derivatized

* Corresponding author. Fax: 5411-4576-3341. E-mail: calvo@q1.fcen.uba.ar.

(1) Bandey, H. L.; Hillman, A. R.; Brown, M. J.; Martin, S. J. *Faraday Discuss.* **1997**, *107*, 105−121.
(2) Calvo, E. J.; Etchenique, R.; Bartlett, P. N.; Singhal, K.; Santamaría, C. *Faraday Discuss* **1997**, *107*, 141−157.
(3) Lucklum, R.; Hauptmann, P. *Faraday Discuss.* **1997**, *107*, 123.
(4) Wolf, O.; Seydel, E.; Johannsmann, D. *Faraday Discuss.* **1997**, *107*, 91−104.
(5) Rodahl, M.; Höök, F.; Fredriksson, C.; Keller, C. A.; Krozer, A.; Brzezinski, P.; Voinova, M.; Kasemo, B. *Faraday Discuss.* **1997**, *107*, 229−246.
(6) Sun, Y.; Sun, J.; Zhang, X.; Sun, C.; Wang, Y.; Shen, J. *Thin Solid Films* **1998**, *327*, 730.
(7) Onda, M.; Lvov, Y.; Ariga, K.; Kunitake, T. *Biotechnology and Bioengineering* **1996**, *51*, 163−167.
(8) Lvov, Y.; Ariga, K.; Ichinose, I.; Kunitake, T. *J. Am. Chem. Soc.* **1995**, *117*, 6117−6123.
(9) Lvov, Y. *Protein Architecture*; Lvov, Y., Mohwald, H., Eds.; Marcel Dekker: 2000, *6*, 125−167.
(10) Bourdillon, C.; Gueris, J.; Moiroux, J.; Saveant, J. M. *J. Am. Chem. Soc.* **1993**, *115*, 12264−12269.
(11) Decher, G. *Science* **1997**, *277*, 1232−1237.
(12) Caruso, F.; Furlong, D. N.; Ariga, K.; Ichinose, I.; Kunitake, T. *Langmuir* **1998**, *14*, 4559−4565.
(13) Forzani, E. S.; Solis, V. M.; Calvo, E. J. *Anal. Chem.* **2000**, *72*, 5300−5307.
(14) Höök, F.; Rodahl, M.; Brzezinski, P.; Kasemo, B. *Langmuir* **1998**, *14*, 729−734.
(15) Janshoff, A.; Galla, H. J.; Steinenn, C. *Angew. Chem., Int. Ed.* **2000**, *39*, 4004−4032.
(16) Rickert, J.; Brecht, A.; Gopel, W. *Anal. Chem.* **1997**, *69*, 1441−1448.
(17) Su, H.; Chong, S.; Thomson, M. *Langumir* **1996**, *12*, 2247−2255.
(18) Cavic, B. A.; Thomson, M. *Anal. Chem.* **2000**, *72*, 1523−1531.
(19) Fawcett, N. C.; Craven, R. D.; Zhang, P.; Evans, J. A. *Anal. Chem.* **1998**, *70*, 2876−2880.
(20) Höök, F.; Kasemo, B.; Nylander, T.; Fant, C.; Sott, K.; Elwing, H. *Anal. Chem.* **2001**, *73*, 5796.

10.1021/ac0157425 CCC: $22.00
Published on Web 06/06/2002

with an osmium complex (PAH−Os) and glucose oxidase (GOx), $(PAH-Os)_n(GOx)_n$ on Au-coated 10 MHz quartz crystals.[2,21−23] The ellipsometric thicknesses of these multilayer films in contact with water were evaluated at three wavelengths, and the thicknesses can be varied stepwise with the number of enzyme adsorption steps.[24]

The electrical representation of a piezoelectric quartz resonator is given by the transmission line model (TLM) of Mason,[25] where the complex input impedance is given by

$$Z = \frac{1}{j\omega C_0}\left[1 - \frac{K^2}{\phi_q}\frac{2\tan(\phi_q/2) - j(Z_S/Z_q)}{1 - j(Z_S/Z_q)\cot(\phi_q)}\right] \quad (1)$$

where K^2 is the quartz electromechanical coupling coefficient, ϕ is the complex acoustic wave phase shift across the quartz, C_0 is the static capacitance of the resonator, $\omega = 2\pi f$ with f the excitation frequency; Z_q is the quartz characteristic impedance $Z_q = \sqrt{(\rho_q \mu_q)}$, ρ_q is the quartz density and μ_q the quartz stiffness, and Z_S is the surface mechanical impedance due to the surface film and viscous liquid in contact with it.

The motional impedance arising from the mechanical motion of the quartz in parallel with C_0[25] is

$$Z_m = \frac{1}{j\omega C_0}\left[\frac{\phi_q}{2K^2\tan(\phi_q/2)} - 1\right] + \frac{\phi_q(Z_S/Z_q)}{4K^2\omega C_0}\left[1 - \frac{j(Z_S/Z_q)}{2\tan(\phi_q/2)}\right]^{-1} \quad (2)$$

The first term in eq 2 represents the unloaded quartz crystal impedance, and the second term, the lumped element surface (LEM) impedance Z_{LEM} given by

$$Z_{LEM} = \frac{\phi_q(Z_S/Z_q)}{4K^2\omega C_0}\left[1 - \frac{j(Z_S/Z_q)}{2\tan(\phi_q/2)}\right]^{-1} \quad (3)$$

Furthermore, near resonance, $\omega \cong \omega_s$, where $\omega_s = 2\pi f_s$, with f_s, the series resonance frequency and N, the harmonic resonance,[26] and if $|Z_S|/Z_q \ll 2\tan(\phi_q/2)$,

$$Z_{LEM} \cong \frac{N\pi}{4K^2\omega_S C_0}\left(\frac{Z_S}{Z_q}\right) = R_S + jX_{LS} \quad (4)$$

The electroacoustic impedance of a lumped-element BVD resonator composed of a viscoelastic film on a quartz crystal immersed in liquid depends on the liquid density (ρ_l) and viscosity (η_l) and the film thickness (d_f), density (ρ_f), and shear (storage G'_f and loss G''_f) moduli. The validity of the LEM equivalent circuit to within 1% of the transmission line model[26] is fulfilled, since the ratio of the surface film and liquid impedance (Z_S) to the quartz crystal impedance (Z_Q) is $Z_S/Z_Q < 0.005$.

If two nonpiezoelectric layers are successively attached to the crystal, the following expression describes the surface impedance.[27]

$$Z_S = \left(\frac{Z_f^*\tanh(k_f d_f) + Z_l^*\tanh(k_l d_l)}{1 + \frac{Z_l^*}{Z_f^*}\tanh(k_f d_f)\tanh(k_l d_l)}\right) \quad (5)$$

where $L_q = N\pi^2/8K^2\omega_S^2 C_0$, and the subscript "f" denotes the viscoelastic film under-layer and "l", the liquid overlayer, respectively. The characteristic film and liquid impedances are, respectively, Z_f^* and Z_l^*, and k_f, the film complex wave propagation constant $k_f = j\omega(\rho_f/G_f)^{1/2}$. The complex shear modulus is $G = G' + G''_i$, and the characteristic impedance of the Newtonian liquid is $Z_l^* = \sqrt{\rho_l \eta_l \omega j} = (1 + j)\sqrt{\rho_l \eta_l \omega/2}$ and $R_l = X_{Ll}$; the characteristic film impedance is $Z_f^* = \sqrt{(G_f\ \rho_f)}$.

If the liquid layer is much thicker than the acoustic wave penetration, then $\tanh(k_l d_l) \rightarrow 1$, and eq 5 becomes

$$Z_S = \left(\frac{Z_f^*\tanh(k_f d_f) + Z_l^*}{1 + \frac{Z_l^*}{Z_f^*}\tanh(k_f d_f)}\right) \quad (6)$$

Inspection of eqs 4 and 6 shows that one can access experimentally to two quantities of the surface impedance, that is, R_S and X_{LS}, but three film material properties, namely, ρ_f, G'_f, and G''_f and the film thickness, d_f, need to be evaluated.[2]

Several approximations have been made on at least two parameters, normally thickness and density or loss tangent, tan $\alpha = G''_f/G'_f$[2,30,31] or constant Faradaic efficiency and constant density during electrodeposition, and the electrical charge has been taken as a measure of the film thickness.[29]

In previous studies, we reported the volume and viscoelastic changes of cross-linked hydrogels made of the same components, PAH−Os and GOx.[30,31] Our new strategy to approach this problem has been to control the film thickness layer-by-layer (LBL) to study the acoustic impedance of controlled and independently measured thickness films.

For this purpose we have built well-organized layer-by-layer self-assembled enzyme films by alternate electrostatic adsorption of PAH−Os and GOx on Au-coated 10 MHz quartz crystals. Under conditions in which the Sauerbrey approximation was valid, the mass of the films and the ellipsometric thickness gave an estimate of the density for films of different structures and layer numbers.[24] Electrochemical oxidation and reduction of the osmium site in the self-assembled films resulted in changes of ellipsometric film thickness and of acoustic impedance of the modified quartz crystal immersed in electrolyte. Under these conditions, we were able

(21) Hodak, J.; Etchenique, R.; Calvo, E. J.; Singhal, K.; Bartlett, P. N. *Langmuir* **1997**, *13*, 2708−2716.
(22) Calvo, E.; Battaglini, F.; Danilowicz, C.; Wolosiuk, A.; Otero, M. *Faraday Discuss.* **2000**, *116*, 47−65.
(23) Calvo, E.; Etchenique, R.; Pietrasanta, L.; Wolosiuk, A. *Anal. Chem.* **2001**, *73*, 1161.
(24) Forzani, E.; Otero, M.; Calvo, E. J.; Lopez Teijelo, M. *Langmuir* **2002**, *18*, 4020−4029.
(25) Lucklum, R.; Behling, C.; Cernosek, R. W.; Martin, S. J. *J. Phys. D: Appl. Phys.* **1997**, *30*, 346−356.
(26) Cernosek, R. W.; Martin, R. W.; Hillman, A. R.; Bandey, H. L. *IEEE Trans. Ultrason., Ferroelectr. Freq. Control* **1998**, *45*, 1399−1407.
(27) Granstaff, V. E.; Martin, S. J. *J. Appl. Phys.* **1994**, *44*, 209−218.
(28) Lucklum, R.; Hauptmann, P. *Electrochim. Acta* **2000**, *45*, 3907−3916.
(29) Hillman, A. R.; Jackson, A.; Martin, S. J. *Anal. Chem.* **2001**, *73*, 540−549.
(30) Etchenique, R. A.; Calvo, E. J. *Electrochem. Commun.* **1999**, *1*, 167−170.
(31) Calvo, E. J.; Etchenique, R. *J. Phys. Chem. B*, **1999**, *103*, 8944−8950.

to estimate the values of storage G' and loss shear G'' moduli for a seven-PAH−Os/GOx-bilayer film.

EXPERIMENTAL SECTION

Instrumentation. Two electrochemical quartz crystal microbalance (EQCM) systems were employed in this study:

(i) A complex voltage divider reported elsewhere[32] was used to measure the resonance frequency and both components of the quartz crystal modified Butterworth−Van Dyke (lumped-element BVD) equivalent circuit. This device operates by applying to the quartz crystal a 10 MHz sinusoidal voltage (5 mV peak-to-peak) generated by a voltage-controlled oscillator (VCO) connected to the D/A output of a Keithley data acquisition system 575. Both input (V_i) and output (V_o) ac voltage moduli were amplified and rectified, and the resulting signals were measured with an A/D converter under computer control. The ratio of the circuit transfer function modulus, that is, $|V_o/V_i|$ as a function of the VCO output signal frequency was fitted to the nonlinear analytical equation of the BVD transfer function,[32] and the equivalent circuit elements L, R, C_0 and C were obtained

$$\left|\frac{V_0}{V_i}\right| = \frac{\sqrt{\left(\omega L - \frac{1}{\omega C}\right)^2 + R^2}}{\sqrt{\left(\omega L - \frac{1}{\omega C} + \frac{\omega L C_0}{C_m} + \frac{C_0}{\omega C C_m} - \frac{1}{\omega C_m}\right)^2 + \left(R + \frac{R C_0}{C_m}\right)^2}} \tag{7}$$

where C_m is a measuring capacitor, typically of 33 pF.

(ii) An HP5100A network analyzer interfaced by an IEEE-488 card (National Instruments GPIB PCIIA) was used to study the quartz crystal admittance spectrum with a software written for this application under Labview (National Instruments) environment. The conductance Y' and susceptance Y'' of the piezoelectric quartz crystal resonance were synchronously measured with the HP5100A in the transmission mode through a custom-made fixture as a function of the frequency around the series resonance frequency, f_s ($\omega_s = 2\pi f_s$) at which the motional reactance is zero. A three-step calibration of the HP5100A network analyzer was performed for open-circuit, short-circuit, and 50 Ω reference.

Simultaneous fit of the admittance spectra to the conductance Y' and susceptance Y'' for the modified lumped-element BVD equivalent circuit equations using a Levenberg−Marquardt routine written in Labview environment were performed,

$$Y = Y' + jY'' \tag{8}$$

with

$$Y' = \frac{R}{R^2 + \left(\omega L - \frac{1}{\omega C}\right)^2} \tag{9}$$

and

$$Y'' = \omega C_0 - \frac{\left(\omega L - \frac{1}{\omega C}\right)}{R^2 + \left(\omega L - \frac{1}{\omega C}\right)^2} \tag{10}$$

where C_0 is the resultant of the parallel of the static capacitance of the quartz with the stray capacitance of the connections, and L and R are the inductance and damping resistance, respectively, of the motional arm in the lumped element BVD equivalent circuit. The value of the quartz compliance in the motional arm, C, was determined in an initial four-parameter fit and then held constant during fitting of the rest of the data.

Typical values of $R_q = 40$ Ω (including O-ring and crystal fitting), $L_q = 8.5$ mH, $C_q = 30$ fF, and $C_0 = 5$ pF for 10 MHz crystals in air with ωL (total) ≈ 535 000 Ω were obtained.

The frequency corresponding to Y'_{max}, was automatically found by the program and used as the initial value of f_s, and $1/Y'_{max}$ was used as the initial value of R during fitting iterations. The fitting iterations could be completed within ∼ 1.5−3.0 s for a group of 201−501 Y' and Y'' data points when the relative sum of the residual square, q_r, as given in eq 11, had become minimum. The electroacustic impedance parameters were obtained from a fitting procedure in which the whole experimental curves (Y' vs f and Y'' vs f) were considered

$$q_r = \frac{\sum_1^N (Y'_{fit} - Y'_{exp})^2 + \sum_1^N (Y''_{fit} - Y''_{exp})^2}{\sum_1^N Y'_{exp} + \sum_1^N Y''_{exp}} \tag{11}$$

where the subscripts, "fit" and "exp", denote fitted and experimental results.

In both cases i and ii, AT-cut quartz crystals (10 MHz) of 14-mm-diameter (International Crystal Manufacturing Co. Inc., Oklahoma City, OK) of 0.196-cm^2 area were employed.

Both passive methods i and ii employed in the present investigation, voltage divider and network analyzer, provide complementary advantages for the assessment of quartz crystal impedance near resonance: The latter gives complete information on impedance/admittance at resonance frequency and higher harmonics, and the former is a low-cost technique that gives only information on the transfer function modulus but allows much faster data collection.

Chemicals. In the course of the experiments, the following chemicals were used as supplied: sodium 3-mercapto-1-propane sulfonic acid (MPS) (Aldrich), KNO_3 (Merck), Tris (Sigma). Glucose oxidase (GOx) (EC 1.1.3.4) from *Aspergillus niger* was a gift from MediSense, U.K.

The soluble redox mediator, $(Os(bpy)_2ClPyCOOH)Cl$, and the redox polymer $Os(bpy)_2ClPyCH_2NH$poly(allylamine), PAH−Os, were synthesized as previously reported.[33] This polymer solution was purified by dialysis against water for 3 days. The osmium content was evaluated spectrophotometrically at $\lambda = 475$ nm (ϵ

(32) Calvo, E. J.; Danilowicz, C.; Etchenique, R. *J. Chem. Soc., Faraday Trans.* **1995**, *91*, 4083−4091.

(33) Danilowicz, C.; Cortón, E.; Battaglini, F.; Calvo, E. J. *Electrochim. Acta* **1998**, *43*, 3525.

$= 8100\ M^{-1}$) and the number of Os-modified polymer/monomer unit (1:8) was determined by NMR spectroscopy.

Electrochemical Experiments. A standard three-electrode electrochemical cell made of PTFE was used with an operational amplifier potentiostat with the working electrode (Au-coated quartz) at real ground. This Au-coated quartz electrode was simultaneously one of the quartz polarizing contacts at 10 MHz and the electrochemical working electrode. Two vinyl O-rings were used for sealing the quartz crystal, with only one face of the crystal in contact with the electrolyte. The dc circuit, including the potentiostat, was isolated from the 10 MHz ac circuit by a 10 μF decoupling capacitor.

The reference electrode was $Ag/AgCl/Cl^-$, and all potentials herein are quoted with respect to this electrode. A 1 cm^2 platinum mesh was used as the counterelectrode. All electrochemical experiments were carried out in a pH 7.5 buffer solution of 0.010 M Tris with 0.2 M KNO_3.

Self-Assembly Process. The adsorption times for each component, thiol, polymer, and enzyme were determined by a preliminary QCM study.[23]

Thiol Adsorption. Thiol solutions were freshly prepared before each adsorption experiment in order to avoid oxidation in air. The MPS thiol monolayer was formed by soaking Au electrodes in aqueous solutions of 0.02 M sodium 3-mercapto-1-propane sulfonate in 0.01 M H_2SO_4 for 30 min. The Au samples were removed from the adsorption solution and thoroughly washed in distilled water.

PAH−Os Adsorption. The poly(allylamine) osmium derivative was adsorbed onto the thiol-modified gold from 0.4% w/v aqueous solutions of pH 7−8 for 5 min. After adsorption, the modified electrodes were thoroughly rinsed with distilled water.

Enzyme Adsorption. Glucose oxidase was adsorbed for 10 min onto the PAH−Os-modified Au from an aqueous solution containing 1 μM enzyme in water.

RESULTS AND DISCUSSION

In our previous communications,[21,23] we employed the quartz crystal microbalance, QCM, to monitor the stepwise adsorption of GOx on multilayer structures terminated in the Os-containing polycation PAH−Os during adsorption from aqueous solutions of the negatively charged protein.

Multiple protein layers can be assembled on polycationic poly(allylamine) surfaces by reversing the surface charge in every adsorption step upon sequential immersion of the electrode surface in aqueous solutions of redox polyelectrolyte and enzyme, respectively.

Figure 1 depicts a schematic representation of a $(PAH-Os)_n(GOx)_n$ multilayer on a thiolated Au surface according to ellipsometric results of film thickness for the successive layers deposited by electrostatic self-assembling.[24] After a few irregular layers, the thickness increases by the same amount per bilayer deposited, and the multilayer structure results from the electrostatic interaction of negatively charged GOx and positively charged PAH−Os. It should be noted that the interlayer thickness after the fourth PAH−Os/GOx bilayer (48 nm/bilayer) is much larger than the protein molecular size (~4.0 × 5.0 × 7.0 nm) as a result of loops and tails of the polymer at the surface where GOx adsorbs.

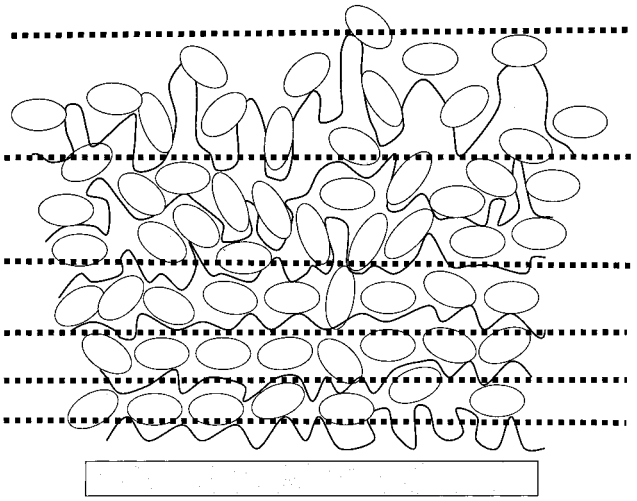

Figure 1. Schematic representation of self-assembled $(PAH-Os)_n(GOx)_n$ multilayers on thiolated gold electrode. Continuous lines represent PAH−Os trails, and ovals represent GOx molecules.

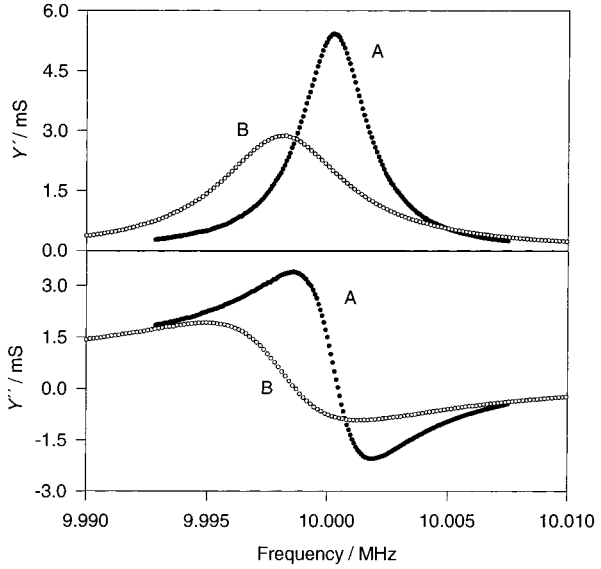

Figure 2. Real and imaginary components of the electrical admittance vs frequency for a 10 MHz TSM resonator crystal coated with Au and MPS and modified with $(PAH-Os)_7(GOx)_7$ self-assembled multilayer: (A) in air and (B) under water.

Admittance spectra around resonance at 10 MHz for a thiolated Au-coated quartz crystal modified with seven successive layers of self-assembled $(PAH-Os)_7(GOx)_7$ dry thin film in air are shown in Figure 2A. The same film immersed in water is shown in Figure 2B. The resonance admittance of the film in contact with the viscous liquid decreases, with broadening of the admittance curve and a shift of the resonance frequency to lower values. The complex surface admittance of the composite resonator is determined by the surface thin film and the viscous liquid, since the shear wave penetrates the ultrathin film (d_f = 217 nm) and is further attenuated in the viscous liquid.

A shift of the resonance frequency, f_s, toward lower values is apparent in successive adsorbed layers, and both peak height and peak width change during the stepwise adsorption. The resonance admittance curve changes during the adsorption of different number of layers reflecting mass increase and energy storage and losses during the shear wave perturbation. The resonance

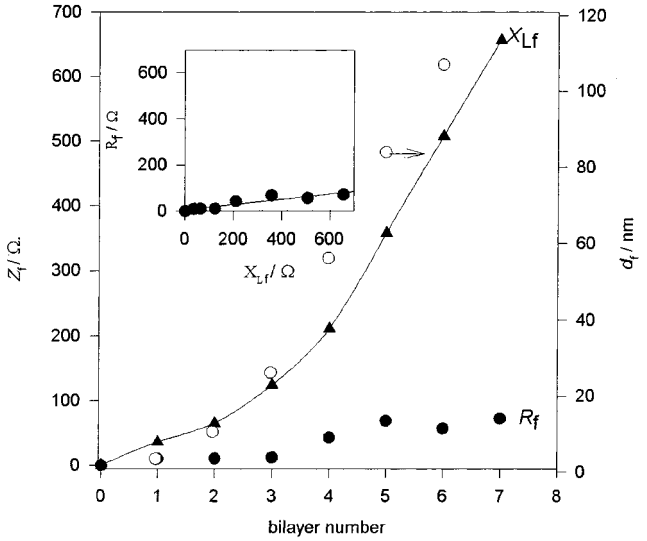

Figure 3. Variation of dry film impedance parameters X_{Lf} and R_f in air as a function of the number of PAH−Os and GOx bilayers, as compared to the ellipsometric film thickness for dry films in air. Inset: parametric plot of R_f vs X_{Lf}.

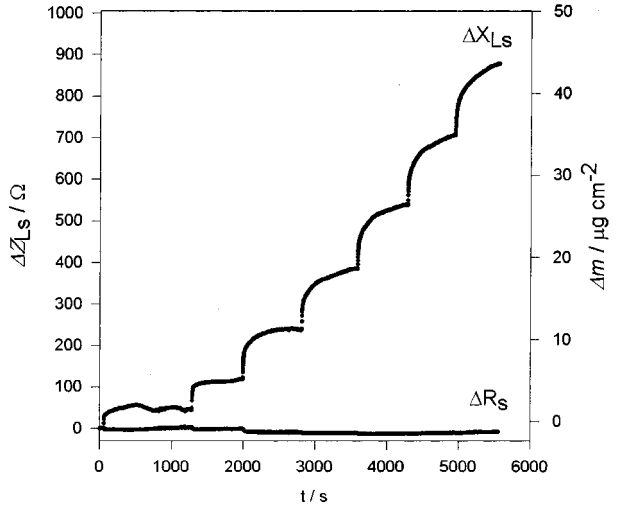

Figure 4. Time evolution of ΔX_{LS} and ΔR_S for a TSM resonator crystal modified with Au/MPS/(PAH−Os)$_{n+1}$(GOx)$_n$ after addition of 11 μL of 11 μM GOx to 220 μL of water (final GOx concentration = 1 μM) for consecutive adsorption of GOx and the corresponding acoustic mass uptake.

frequency shift with further deposited layers corresponds to an increase in mass for acoustically thin films at 10 MHz; however, the increase in peak width with the number of layers also indicates energy dissipation by the thin film.

For the dry film in air, the acoustic impedance grows with the number of layers and follows a trend very similar to the film ellipsometric thickness (Figure 3). A linear dependence of X_{Lf} ($= \omega L_f$) versus d_f yields an average density of 2 g cm^{-3} for the dry film in air. The film motional resistance change, ΔR_f, which reflects shear energy losses in the film, also increases with the number of deposited enzyme−polymer pairs of layers, because it was experimentally difficult to eliminate the trapped water from the film because of the hydrophilic nature of proteins and poly(allylamine). However, the ΔR_f increment was always much less than the inductive impedance changes, ΔX_{Lf}. Furthermore, the inset in Figure 3 shows a parametric plot from which it can be seen that $\partial R_f / \partial X_{Lf}$ is very small, and therefore, the film in air can be taken as acoustically thin.

For dry films, the mass per enzyme layer result is 1.67 μg cm^{-2} for the first layer (8.98×10^{-12} mol cm^{-2} of GOx), which is larger than that expected for a closely packed GOx from crystallographic data, namely, 4.6×10^{-12} mol cm^{-2}. For a film with two and three layers, we find 3.01 μg cm^{-2} (16.2×10^{-12} mol cm^{-2}) and 5.77 μg cm^{-2} (31.0×10^{-12} mol cm^{-2}), respectively. After the third enzyme layer, a constant mass increase per layer of 6.9 μg cm^{-2} (37.1×10^{-12} mol cm^{-2}) is obtained (Figure 3).

The increase in film roughness with the number of layers that results from looping of the poly(allylamine) may explain the excess enzyme mass, as is the case for the ellipsometric thickness.[24] The excess mass may also be due to the fact that the enzyme is never completely dehydrated and also due to the presence of counterions that neutralize ionized carboxylate and amine groups.

The time course of the quartz crystal impedance change ($\Delta Z_{LS} = Z_{LS}(t) - Z_{LS}(t = 0)$) during adsorption of GOx from aqueous solutions on PAH−Os-terminated layers has been studied by precise time-resolved measurements of the frequency shift and the energy dissipation motional resistance R_S, of the composite quartz |film| liquid resonator. Figure 4 shows the time course of ΔZ_{LS} during GOx consecutive adsorption steps for a seven-GOx-layer film immersed in aqueous solution. The values of ΔR_S are always smaller than the values of ΔX_{LS}, so the Os(II) film in contact with the electrolyte can be regarded as acoustically thin, and the decrease in the resonance frequency (or increase in ΔX_{LS}) can be taken as a measure of the mass increase during the protein adsorption.

Although ΔX_{LS} increases with the number of layers, in some experiments, a small decrease in ΔR_S upon adsorption of GOx on the PAH−Os-terminated surface has been observed in the first layers. This decrease in acoustic energy dissipation must be associated with adsorption of GOx on a dissipative nonrigid polymer surface, forming a more compact structure.[20] In Figure 4, for more than four layers, ΔR_S increases steadily upon adsorption of GOx with respect to the PAH−Os-terminated layer; thus, the effect of multilayer thickness prevails.

For the oscillation of the thin polymer film in air, the acoustic wave amplitude damps rapidly to 0 at the air−polymer interface. In liquid, on the other hand, the lossy polymer may extend into the electrolyte, dissipating energy under shear perturbation. The acoustic wave penetrates several hundred nanometers into the liquid and, therefore, probes a longer distance in water than in the dry film. During protein adsorption on the polyelectrolyte modified surface, strong electrostatic interaction between the polymer and the enzyme produces a more compact layer by displacing counterions and solvent entrained by the polymer segments and results in less dissipation under shear perturbation than for the PAH−Os-terminated surface.[16,35] After several enzyme layers have been deposited, the energy dissipation increases because of the thicker film, and thus, the motional resistance increases with the amount of deposited enzyme.

Both ellipsometric thickness and gravimetric QCM measurements reveal that the self-assembled PAH−Os/GOx multilayers

(34) Ladam, G.; Gergely, C.; Senger, B.; Decher, G.; Voegel, J. C.; Schaaf, P.; Cuisinier, F. J. G. *Biomacromolecules* **2000**, *1*, 674−687.
(35) Donath, E.; Walther, D.; Shilov, V. N.; Knippel, E.; Budde, A.; Lowack, K.; Helm, C. A.; Möhwald, H. *Langmuir* **1997**, *13*, 5294−5305.

are highly hydrated in contact with water (see below). Probably the films dried under a N_2 stream contain considerable amounts of residual water, since poly(allylamine) is highly hygroscopic, and it is well-known that proteins retain water in their structure.

For the film in contact with aqueous electrolyte, once the GOx overlayer has been added, the steady-state mass is 35% larger than for the same dry film,whereas the hydrated film thickness doubles the value of the dry film. Gopel et al. reported that the QCM frequency shift of rigid protein films immersed in aqueous electrolyte is 4−5 times larger than the values found for the same films under dry conditions.[16] It has been suggested that the excess mass is due to solvent molecules and ions associated with the protein.

It should be noted that the film thickness values derived from acoustic and optical measurements do not coincide, since water molecules that are not polarized in the visible spectral region are not detected in reflectance methods, unlike the shear wave that senses water in the film as a coupled mass. The acoustic contrast between the film and liquid depends on the difference in shear modulus (i.e., $>10^6$ Pa for the film and 10^4 Pa for water), and this is more pronounced than the optical contrast given by the difference in the refractive index of the hydrated film and water (~1.43 for the protein film and 1.33 for water). Therefore, the most highly hydrated outer regions of the film cannot be distinguished from the aqueous electrolyte by the optical methods but can be detected by the acoustic wave.

One can derive an ellipsometric areal mass density, Δm_e from the optical film thickness (d_f) and film refractive index (n_f) through the equation proposed by Feijter et al.,

$$\Delta m_e = d_f \frac{n_f - n_0}{\partial n / \partial c} \tag{12}$$

where n_0 is the electrolyte solution refractive index; n_f, the film refractive index; and $\partial n/\partial c$ is the refractive index increment of the adsorbed substance measured in solutions of GOx, $\partial n/\partial c = 0.177$ cm^3 g^{-1}.

Since the ellipsometric thickness measurement would overestimate the film density, Höök and Kasemo[20] have represented the protein film with an effective hydrodynamic thickness, d_{eff} and an effective density, ρ_{eff}. The effective thickness can be expressed in terms of the Sauerbrey mass, Δm_{QCM}; the ellipsometric mass, Δm_e; and the respective densities of the dry protein film, $\rho_{dry} = 2.0$ g cm^{-3} and water, ρ_{water}, as follows.

$$d_{eff} = \frac{\Delta m_{QCM}}{\rho_{eff}} = \frac{\Delta m_{QCM}}{\rho_{dry}\frac{\Delta m_e}{\Delta m_{QCM}} + \rho_{water}\left(1 - \frac{\Delta m_e}{\Delta m_{QCM}}\right)} \tag{13}$$

The effective thickness is always larger than the ellipsometric thickness and smaller than the QCM thickness, as depicted in Figure 5. In the first layers, the effect of the fluffy or "hairy" external film|water structure, which cannot be seen by ellipsometry, becomes dominant, and as more layers are built up, the effect of the interface with the external electrolyte is less important.

Since the reduced Os(II) films can be regarded as acoustically thin, we can estimate the film's effective density from the

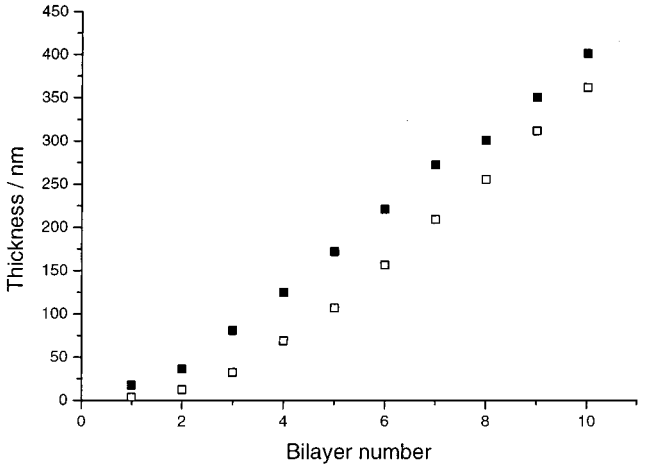

Figure 5. Effective thickness calculated with eq 13 (■) and ellipsometric thickness (□) as a function of the number of PAH−Os/GOx pair of layers. Other conditions as in Figure 4.

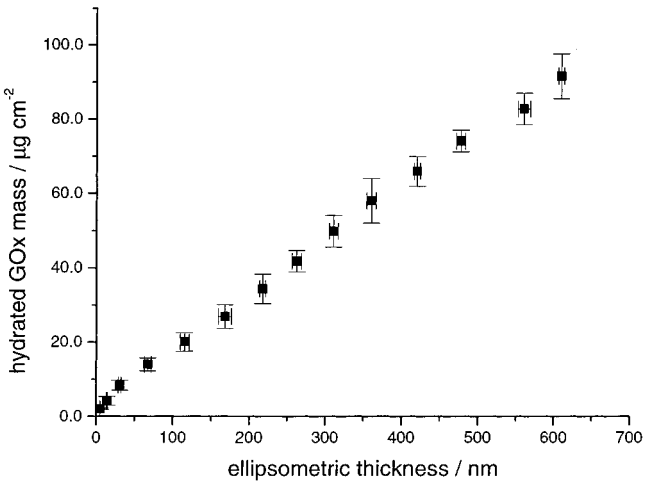

Figure 6. Plot of hydrated GOx mass vs ellipsometric film thickness for Au/MPS/(PAH−Os)$_n$(GOx)$_n$ ($1 \le n \le 14$) in contact with water.

gravimetric mass obtained from the Sauerbrey equation combined with the ellipsometric thickness. A comparison of the QCM GOx mass versus the ellipsometric thickness for films exposed to liquid is shown in Figure 6. From the slope, an average density of 1.7 ± 0.2 g cm^{-3} after the fourth layer was obtained. It should be noted that this film density is probably overestimated, since the ellipsometry underestimates the film thickness.

A unique calculation of the shear parameters requires knowledge of the film thickness (d_f) and film density (ρ_f), because multiple combinations of the coating parameters produce similar admittance spectra.[36,37] The electroacoustic impedance of a lumped-element BVD resonator composed of a viscoelastic film on a quartz crystal immersed in liquid depends on the liquid density and viscosity and the film thickness, density, and shear (storage and loss) moduli. Therefore, one can access experimentally two quantities of the surface impedance, that is, R_S and X_{LS} (or Δf_s), but three film material properties and the film thickness need to be evaluated. For this reason, in previous work with hydrogels of PAH−Os and GOx,[31] we made several approxima-

(36) Arnau, A.; Jiménez, Y.; Sogorb, T. *IEEE Trans. Ultrasound, Ferroelectr. Freq. Control* **2001**, *48* (5), 1367−1382.
(37) Behling, C.; Lucklum, R.; Hauptmann, P. *Sens. Actuators* **1997**, 260−266.

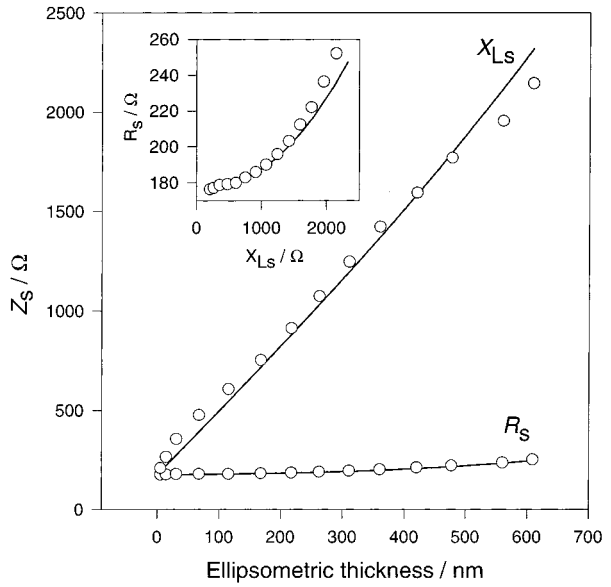

Figure 7. Experimental data (open circles) and simulations of X_{LS} and R_S (solid line) layers of (PAH−Os)$_{14}$(GOx)$_{14}$ under water with $G_f' = 9.9$ MPa, $G''_f = 0.7$ MPa, $\rho_f = 1.5$ g cm^{-3} and $\rho_{H_2O} = 1$ g cm^{-3} and $G''_{H_2O} = \omega\eta_l = 6 \times 10^4$ Pa. Inset: Parametric plot of R_S vs X_{LS} and simulation (solid line).

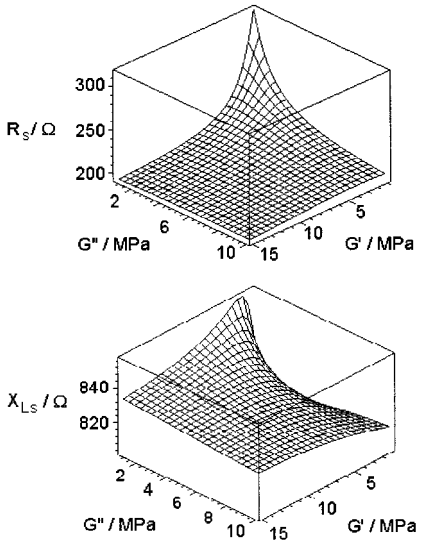

Figure 8. Real (R_S) and imaginary (X_{LS}) parts of the acoustic impedance at 10 MHz of a quartz crystal modified with (PAH−Os)$_7$(GOx)$_7$ film in contact with water electrolyte of $\rho = 1$ g cm^{-3} and $G'' = 6 \times 10^4$ Pa, for $d_f = 300$ nm as a function of shear storage modulus G'_f and loss modulus G''_f at 10 MHz, calculated with eqs 4 and 5.

tions on at least two parameters, namely, thickness and density, or the loss tangent of the film, tan $\alpha = G''_f/G'_f$, at the resonance frequency.

The quartz electrical impedance for a viscoelastic film in contact with a viscous fluid is given by eqs 4 and 5, derived by Granstaff and Martin,[27] for multiple nonpiezoelectric viscoelastic overlayers on a quartz crystal resonator. For the bare quartz crystal immersed in water, the values of the impedance components at 10 MHz are the same, $R_l = X_{Ll} = 178$ Ω (see Figure 7 for $d_f = 0$).

Equation 5 cannot be transformed analytically into an explicit form of the shear modulus. To extract film shear modulus from quartz crystal electroacoustic impedance, a complex data-fitting procedure must be employed. The entire complex admittance spectrum has to be calculated for each guess of the shear parameters and then compared to the measured values. From eq 5, we can estimate G'_f and G''_f by a root-finding method, which calculates values of X_{LS} and R_S from a range of trial values of G'_f and G''_f in a given range for fixed values of d_f and ρ_f. Then these impedance values are compared to experimental data, and the error is calculated; this procedure is repeated until the error in both complex impedance components falls within the preset values.

Instead of using the root-finding procedure, we have calculated surface plots for X_{Lf} and R_f using eqs 4 and 5 for a fixed film thickness and density as a function of G'_f and G''_f. It can be seen in Figure 8 that for most of G'_f and G''_f values in the range considered, there is a very weak dependence of the impedance components, and within the experimental error in the determination of X_{Lf} and R_f, a large set of values of shear moduli would result in the inversion process. Moreover, the extraction of the shear moduli is very sensitive to the choice of the film thickness value, and slight differences in d_f may produce very different values for G' and G''.

The values of the viscoelastic moduli, G' and G'', used in the simulation of the experimental data in Figure 7 result in the MPa range, even though no exact evaluation could be made, since the shear moduli can be varied within a large range with a very small variation of the surface impedance (see 3D plots in Figure 8). For the values of G' and G'' that correspond to the whole data set in Figure 7, there is little variation, and hence, small differences in the experimental impedance values lead to very large variations of G' and G'' when inverting eq 5, because the system is near the acoustically thin regime.[2,28,36]

Since the reduced Os(II) films under water and dry films are acoustically thin, it is not possible to assess exact values of G'_f and G''_f moduli, and the acoustic impedance can be ascribed to a good approximation to an increase in film thickness every time a new overlayer is added. We can calculate X_{LS} and R_S for the successive PAH−Os/GOx layers with eq 5. Figure 7 shows the experimental surface impedance data for 14 consecutive enzyme bilayers and the calculated values of X_{LS} and R_S using $\rho_f = 1.7$ g cm^{-3}, the film ellipsometric thickness and the liquid density and viscosity, with constant values of $G'_f = 9.8$ MPa and $G''_f = 0.7$ MPa for the whole multilayer structure (solid line). Note that a single set of G', G'', and ρ_f were used to simulate the whole set of experimental data for the surface acoustic impedance and that the discrepancy between experimental and simulated data for low and high thickness may result in slight changes in the viscoelastic parameters with thickness not taken into account in the simulation.

The values of X_{LS} and R_S increase with the number of deposited PAH−Os/GOx pairs of layers, that is, with the film thickness at constant density. The inset in Figure 7 is a parametric plot of R_S vs X_{LS} for the experimental impedance data, and the solid line, calculated with eqs 4 and 5 and the above film parameters. It is rewarding to observe the good agreement with the viscoelastic model given the approximation of constant density and shear moduli and films of different thicknesses.

The self-assembled layer-by-layer enzyme thin films behave as a viscoelastic film at 10 MHz, where the ionic atmosphere relaxation of ionized groups are responsible for sound absorption that reflects in the storage modulus, and the friction of ions and solvent with the moving polymer chains are responsible for the loss modulus.

Under a sinusoidal perturbation, the ions in the polyelectrolyte at the surface possess an oscillatory motion around their equilibrium positions. At low frequency, the ionic atmosphere associated with a polyion has an asymmetry as a result of the external force balanced by internal friction with the solvent. At higher frequencies when the ionic atmosphere relaxation time, τ, is such that $\omega\tau \approx 1$, then the asymmetric ionic atmosphere has less chance to be formed. This is expected to occur in the MHz frequency range where the QCM works. Finite reorientation time, τ, of molecules under shear stress characterize Maxwellian fluids,[38]

$$\eta = \frac{\eta_0}{1 + j\omega\tau} \tag{14}$$

with η_0 the low-frequency viscosity. For $\omega\tau \ll 1$ $\eta(\omega) \rightarrow \eta_0$, for $\omega\tau \approx 1$ on the other hand, the elastic energy is not totally dissipated in viscous flow, and some is stored elastically by the polymer. It should be noted that the present study refers to a single frequency in the 10 MHz range.

In the reduced state, the Os(II) polymer, $(PAH-Os)_n(GOx)_n$ multilayers with $n \leq 14$ in contact with electrolyte behave as acoustically thin films, and the increase in surface acoustic impedance corresponds simply to an increase in the hydrated film thickness. When the films are switched between reduced (PAH−Os(II)) and oxidized (PAH−Os(III)) states, however, a pronounced change in the complex surface acoustic impedance is observed, as shown in Figure 9 under triangle wave potential perturbation between 0.00 and 0.50 V. An increment of 5% in X_{LS} and 12% in R_S upon osmium oxidation in the film is observed and a corresponding decrease when the Os(III) films are reduced. The ellipsometric thickness increases under similar conditions by 10% (from 330 nm in the reduced state to 365 nm in the oxidized state) during these transformations. The variations of X_{LS} and R_S during film oxidation are due not only to film thickness, since simulations with eq 5 for these thicknesses and density (1.7 g cm^{-3} which remains constant within 2.9% from the variation in the refractive index) predict values of X_{LS} and R_S in defect with respect to the experimental data.

The resulting values of the shear moduli for $(PAH-Os)_7(GOx)_7$ are summarized in Table 1. Although the storage modulus remains almost unchanged, the loss modulus increases almost five times for the fully oxidized Os(III) film. This corresponds to the ingress of anions and solvent with swelling of the film resulting in an increase in the friction of polyions with the solvent and a larger concentration of small counterions. A detailed study of the acoustic impedance of these films in contact with aqueous electrolyte during oxidation and reduction under voltammetric and chronoamperometric conditions is reported in a separate communication.[40]

(38) Ferry, J. D. *Viscoelastic Properties of Polymers*, 3rd. Ed.; Wiley: New York, 1980.

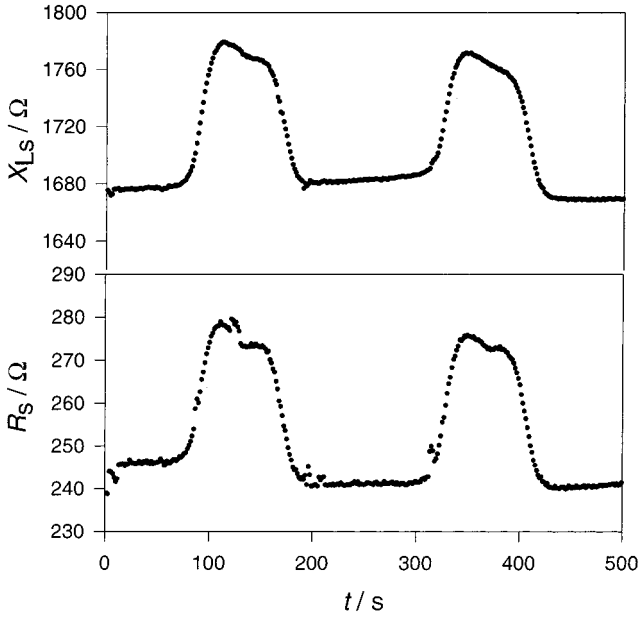

Figure 9. Time evolution of X_{LS} and R_S during oxidation and reduction of PAH−Os in a $(PAH-Os)_7$ $(GOx)_7$ thin film immersed in 0.20 M KNO_3 and 0.01 M Tris electrolyte of pH 7.5 as the electrode potential was varied linearly between 0.00 and 0.50 V at 4 mV s^{-1}.

Table 1. Shear Moduli at 10 MHz for Reduced and Oxidized Films

redox state	G''_f, MPa	G'_f, MPa	$\lvert G_f \rvert$, MPa
fully reduced	1.1	5.9	6.0
fully oxidized	5.2	4.8	7.1

According to Hillman and Martin,[29] the shear wave acoustic decay length, δ, for a TSM resonator is given by

$$\delta = \frac{1}{\omega\sqrt{\rho_f}}\sqrt{\frac{2|G|}{1 - G'/|G|}} \tag{15}$$

Although the acoustic decay length is 180 nm for water at 10 MHz, using values of shear modulus from Table 1 and eq 15, we obtain an acoustic decay length of 11 μm for the reduced Os(II) films ($d_f = 0.33$ μm) and 2.7 μm for the oxidized Os(III) film ($d_f = 0.37$ μm). It is noteworthy that the values derived here are not very different from those recently reported by Hillman and Martin[29] for poly(3-methylthiophene) films of $d_f \approx 0.5$ μm and $\rho_f = 1.09$ g cm^{-3}, with $G' = 2.3$ MPa and $G'' = 2.0$ MPa, characteristic of viscoelastic films with an acoustic decay length of 2.4 μm. The magnitude found for the shear moduli is also in the range previously reported for much thicker hydrogels and 2 orders of magnitude larger than for pure water, $G'' \sim 6 \times 10^4$ Pa.

The film thickness in the reduced state is much less than the shear wave penetration depth, resulting in acoustically thin films, whereas the Os(III) films behave very similarly to viscoelastic poly(3-methylthiophene) films[29] with $d_f/\delta = 0.10-0.20$.

CONCLUSIONS

Electroacoustic parameters have been obtained for electrostatically self-assembled, ESA, $(PAH-Os)_n(GOx)_n$ films both in

(39) Calvo, E. J.; Forzani, E.; Otero, M. Acoustic Wave Sensor Workshop, Taos, New Mexico, August 2001.
(40) Calvo, E. J.; Forzani, E.; Otero, M. *J. Electroanal. Chem.*, submitted.

air (X_{Lf} and R_F) and in contact with water (X_{LS} and R_S) during the layer-by-layer buildup. The electrostatically self-assembled enzyme multilayers behave as viscoelastic films at 10 MHz with G' and G'' on the order of 10^6 Pa in the reduced Os(II) state. However, the films investigated for as many as 14 bilayers are much thinner than the shear wave attenuation in the film and adjacent liquid electrolyte for film thickness below 600 nm. Therefore, the Sauerbrey equation can be used for gravimetric evaluation of film growth.

The resulting mass and ellipsometric thickness increase with the number of layers. An effective film density for the multilayer was estimated for films with more than 3−4 layers with a constant average value of $\rho_f = 1.7 \pm 0.2$ g cm^{-3}, which is probably an overestimate.

For the oxidized films, on the other hand, an increase in R_S and X_{LS} with the number of (PAH−Os)(GOx) bilayers has been observed, as is described in detail elsewhere.[40] This fact is a direct consequence of the ingress of anions and solvent during film oxidation, which results in an increase in the friction of polyions with the solvent and a larger concentration of small counterions.

ACKNOWLEDGMENT

E. Forzani and M. Otero thank CONICET for a postdoctoral and a doctoral fellowship, respectively. Financial support from University of Buenos Aires, CONICET and ANPCyT are gratefully acknowledged. E. J. Calvo acknowledges a Guggenheim Fellowship 2001.

Received for review December 18, 2001. Accepted April 29, 2002.

AC0157425